第44卷第1期 中国科学技术大学学报 Vol. 44, No. 1
2014年1月 JOURNAL OF UNIVERSITY OF SCIENCE AND TECHNOLOGY OF CHINA Jan. 2014

Article ID:0253-2778(2014)01-0048-13

Subspace interference alignment on Grassmann manifold for cellular networks

ZHANG Chen, YIN Huarui, LI Xu, WEi Guo

(*WINLab, University of Science and Technology of China, Hefei* 230027, *China*)

Abstract: The subspace interference alignment for multi-cell and multi-user cellular networks was focused. Different from most previous algorithms that are based on a joint design of precoder and receive filter, the proposed method achieves interference alignment with precoder design only. This means our algorithm only requires the participation of transmitters, which will alleviate significantly the overhead induced by alternation between the up and down links. More importantly, varying from the traditional constrained optimization method, the precoder design on complex Grassmann manifold with lower dimensions was reformulated and a novel steepest descent algorithm was derived to achieve perfect subspace interference alignment. Simulation results suggest that the proposed algorithm has better convergence performance and higher system capacity compared with previous methods.

Key words: interference alignment; MIMO; cellular networks; Grassmann manifold; optimization; precoder

CLC number: TN92 **Document code**: A doi:10.3969/j.issn.0253-2778.2014.01.006

Citation: Zhang Chen, Yin Huarui, Li Xu, et al. Subspace interference alignment on Grassmann manifold for cellular networks[J]. Journal of University of Science and Technology of China, 2014,44(1):48-60.

蜂窝网络中基于格拉斯曼流形的子空间干扰对齐研究

张 晨,尹华锐,李 旭,卫 国

(中国科学技术大学无线网络通信实验室,安徽合肥 230027)

摘要:研究了多小区多用户蜂窝网络中子空间干扰对齐技术.与基于预编码与接收滤波器联合设计的传统方法不同,本文提出的方法只需要预编码参与迭代优化,这样能够避免上下行链路反复交替迭代带来的冗余开销.更重要的是我们引入了格拉斯曼流形,将优化问题在此流形上重组,降低了空间维度,提出该流形上的最陡下降沿算法达到子空间干扰对齐.仿真结果表明本文提出的方法比已有算法具有收敛速度快,系统容量高的优势.

关键词:干扰对齐;多输入多输出系统;蜂窝网络;格拉斯曼流形;优化;预编码

Received:2013-03-06;**Revised**:2013-04-18

Foundation item: Supported by National Natural Science Foundation of China (61171112), MIIT of China (2010ZX03005-001-02, 2012ZX03001037, 2010ZX03002-010-02).

Biography: ZHANG Chen, male, born in 1985, 博士生. Research field: 多用户干扰对齐技术. E-mail: zhangzc@mail.ustc.edu.cn

Corresponding author: WEI Guo, PhD/Professor. E-mail: wei@ustc.edu.cn

0 Introduction

Interference alignment (IA)[1-2] as a novel MIMO transmission technique has attracted emerging attention recently. It can achieve much higher wireless network capacity than previously believed[3]. The main idea of IA is to design the precoders in a way that at a particular receiver its signals and interference are separated spatially and all of the interference will be overlapped within a designed direction or space, thus making the signaling space interference-free for the desired signals. By employing subspace interference alignment technique, Suh et al[4] prove that for the case of G-cell with K-mobile stations (MSs) per cell, the sum capacity approaches

$$C_{\text{sum}} = \frac{GK}{(\sqrt[G-1]{K}+1)^{G-1}}\log(1+\text{SNR}) + o(\log(\text{SNR})) \tag{1}$$

and the degrees of freedom (DoF) per cell can be achieved as

$$\text{DoF} = \frac{1}{G}\lim_{\text{SNR}\to\infty}\frac{C_{\text{sum}}}{\log(\text{SNR})} = \frac{K}{(\sqrt[G-1]{K}+1)^{G-1}} \to 1 \quad \text{as} \quad K \to \infty \tag{2}$$

in Refs. [4,5]. And our early works in Refs. [6,7] have derived the DoF region and the corresponding precoder design for the two-cell case.

By employing the channel reciprocity, some previous works such as Refs. [8-13] jointly design precoder and receiver filter through alternating between the forward and reverse links to achieve interference alignment in a distributed way. However, this alternation needs synchronization at each node, which may introduce too much overhead when the channel varies quickly. On the other hand, these previous works[8-13] only focus on the K-user interference channel and are thus not applicable to the cellular networks directly. More importantly, all of their proposed algorithms employ transitional constrained optimization methods in high dimensional complex space which involve high complexity and poor converge performance.

In this paper, we focus on the subspace interference alignment algorithm for multi-cell and multi-user cellular networks. Our work is different from most previous algorithms that are based on a joint design of precoder and receive filter. By restricting the optimization only at the transmitters' side, the proposed method achieves interference alignment with precoder design only. At each receiver, a simple zero-forcing filter is employed to suppress interference. Therefore it will alleviate the redundant overhead generated by alternation between the up and down links More importantly, we introduce complex Grassmann manifold to subspace interference alignment for cellular networks. Our work is not a simple combination of techniques from different realms, however. First by exploring the unitary invariance property of our cost function, we reform the constrained precoder design to an unconstrained and non-degraded optimization problem on complex Grassmann manifold. Then we locally parameterize the manifold by Euclidean projection from the tangent space onto the manifold instead of the traditional method by moving descent step along the geodesic in Refs. [14-17]. Finally a low-dimensional steepest descent (SD) algorithm on this manifold is derived to approach theoretical DoF per cell. Furthermore, numerical simulation shows that the novel low complexity algorithm has better convergence performance and higher system capacity. Finally, we prove the convergence of the proposed algorithms.

Notation: We use bold uppercase letters for matrices or vectors. $\boldsymbol{X}^{\mathrm{T}}$ and $\boldsymbol{X}^{\dagger}$ denote the transpose and the conjugate transpose (Hermitian) of the matrix $\boldsymbol{X}$ respectively. Then $\boldsymbol{I}$ represents the identity matrix. Moreover $\mathrm{tr}(\cdot)$ indicates the trace operation. And the Euclidean norm of $\boldsymbol{X}$ is $\|\boldsymbol{X}\| = \sqrt{\mathrm{tr}(\boldsymbol{X}^{\dagger}\boldsymbol{X})}$. $\lfloor \boldsymbol{X} \rfloor$ denotes the subspace spanned by the columns of $\boldsymbol{X}$. $\mathbb{C}^{n\times p}$ represents the $n\times p$ dimensional complex space assuming $n > p$. $\mathbb{R}^{+}$ represents positive real number space. $\Re\{\cdot\}$

and $\mathcal{R}\{\cdot\}$ denote the real and imaginary parts of a complex quantity, respectively.

1 System model

As well known, the interfering multiple access channel (IMAC) and the interfering broadcast channel (IBC) can be molded for the uplink and downlink of cellular system, respectively. Ref. [4] proved the DoF duality between the IMAC and IBC. Thus, focusing on the IMAC is enough to present our method for IA. Consider the Interfering Multiple Access Channel (IMAC) for mutiple cells depicted in Fig. 1. Assuming there are K mobile stations (MSs) in each cell. And there are G cells in total. Each MS and BS are equipped with M antennas. Finally the received signal vectors at BS ψ after zero-forcing the interference are denoted by:

$$\left.\begin{aligned}\overline{\mathbf{Y}_\psi} = \mathbf{U}_\psi^\dagger \mathbf{Y}_\psi = \mathbf{U}_\psi^\dagger \Big(\sum_{k=1}^{K} \mathbf{H}_{\psi k}^{\psi} \mathbf{V}_{\psi k} x_{\psi k} + \\ \sum_{\sigma} \sum_{k=1}^{K} \mathbf{H}_{\sigma k}^{\psi} \mathbf{V}_{\sigma k} x_{\sigma k} + \mathbf{W}_\psi\Big) \\ \psi, \sigma \in \{\alpha, \beta, \gamma, \cdots\}, \text{ and} \psi \neq \sigma\end{aligned}\right\} \quad (3)$$

where the subscripts and superscripts represent transmitter and receiver sides, respectively. Additionally, $\boldsymbol{H}_{\psi k}^{\sigma}$ denotes the i. i. d. complex Gaussian channel coefficients matrix from the kth MS of cell ψ to BS σ. And all the channel state information is assumed priorly known by the transmitters[1,4]. And $x_{\psi k}$ represents an

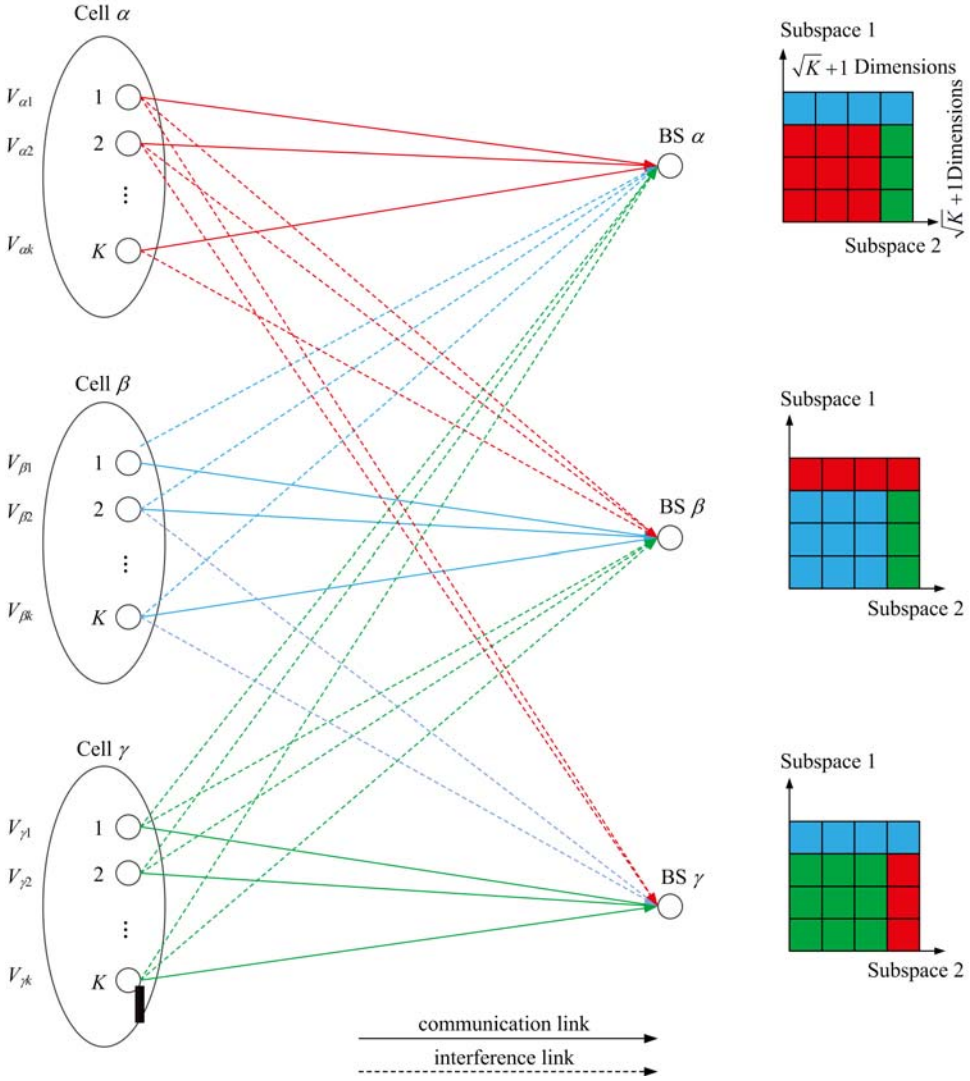

Fig. 1 Subspace interference alignment for three-cell case

independently encoded complex Gaussian symbol with normalized power that beamformed with the corresponding $M\times 1$ precoder vector $\mathbf{V}_{\psi k}$, and then transmitted by the kth MS in cell ψ. $\mathbf{U}_{\psi}$ is a zero-forcing (ZF) filter which projects the desired signal onto the orthogonal space of interference at BS ψ. Obviously, the ZF filter is determined by the interference[4]. Finally $\boldsymbol{W}_{\psi}$ is the i.i.d. complex Gaussian noise with zero mean unit variance.

In addition, if we take the downlink of IBC as our system model, we can obtain similar signal model easily by reversing the roles of the transmitter-receiver pair as well as their corresponding precoder and ZF vectors, because of the duality between up and down link as previously discussed. That is to say if the proposed algorithm fits the precoder of IMAC, its feasibility for IBC is then guaranteed by the duality.

2　Subspace interference alignment and the precoder design

Our previous works in Refs. [6-7] have derived the DoF region and the corresponding precoder design for the two-cell case. However aligning interferences becomes more difficult for the cellular networks (more-than-three-cell case). There are two challenges for interference alignment in cellular networks. First, due to the multiple non-intended receivers (multiple interferes), alignment for one receiver does not ensure alignment at all other receivers. Second, traditional optimization methods of interference alignment involve optimization in high-dimensional complex space, especially for cellular networks. They will suffer from high computational complexity, slow convergence and large residual interference.

By exploring subspace interference alignment[4], we solve the first problem and by introducing optimization on Grassmann manifold, the second challenge is overcome. We will separately present details in this section and the following section.

As previous stated, the simple interference alignment scheme[7] employed in 2IMAC (two-cell-case) can not be applied straight forwardly to cellular networks. That is because different from the two-cell case, aligning interferences into only one dimension or one space will be unfeasible for the cellular networks. Thus we align interferences into multi-dimensional subspace instead of one dimension. Fig. 1 roughly illustrates the concept of subspace interference alignment for the three-cell case (3IMAC). From Eq. (2), it can be obtained that for 3IMAC, the DoF (per cell) is:

$$\frac{K}{(\sqrt{K}+1)^2} \tag{4}$$

which means we must reserve K-dimensional subspace for the desired signal of the $(\sqrt{K}+1)^2$-dimensional total space at each BS. Suppose that the $(\sqrt{K}+1)^2$-dimensional total space is decomposed into two $\sqrt{K}+1$-dimensional subspaces such that the product of each subspace's dimension is the dimension of the total space. If K is not a square number, the dimensions of signal subspace $\sqrt{K}$ is not a integer. We can use time extension to extent a symbol to T time slots, making TK a square number[1]. Thus the dimensions $\sqrt{TK}+1$ will become a integer number to make the subspace interference feasibility.

Similarly, the corresponding precoder vector is composed into two subspace vectors. Generally speaking, the key idea of subspace interference alignment is to design subspace 1 vectors to achieve subspace 1 alignment at one receiver, and subspace 2 vectors for subspace 2 alignment at the other receiver. As shown in Fig. 1, we design corresponding subspace 1 vectors of MSs in cell β so that the interference from cell β spans only one dimension of subspace 1 (subspace 1 alignment) but $\sqrt{K}+1$ dimensions of subspace 2 at BS α. At the same time we design subspace 2 vectors of MSs in cell γ for subspace 2 alignment so that the interference from cell γ spans only one dimension

of subspace 2 so that it also $\sqrt{K}+1$ dimensions of subspace 1. Finally for the desired signals from cell α, no spaces are aligned, therefore they span $\sqrt{K}$ interference-free dimensions of subspace 1 and $\sqrt{K}$ dimensions of subspace 2. Totally, the inter-cell interference from cell β is aligned into one dimension of subspace 1, and distinct at subspace 2, thus it spans $(\sqrt{K}+1)\times 1$ dimensions in all, the same dimension size as interference from cell γ. On the other hand, the desired signals from cell α occupy the reserved $\sqrt{K}\times\sqrt{K}=K$ dimensions. Similar idea is employed at each cell to align interference. The details of subspace interference alignment can be found in Ref. [4].

Therefore the question is how to design feasible subspace precoder vectors to achieve subspace interference alignment in realistic wireless channels. Suh et al proved that for both single-path random delay channel and multi-path frequency-selective channel, the channel coefficient matrix $\boldsymbol{H}\in\mathbb{C}^{M\times M}$ can be N-level decomposed as

$$\boldsymbol{H}=\bigotimes_{n=1}^{N}\boldsymbol{H}^{n}=\boldsymbol{H}^{N}\otimes\boldsymbol{H}^{N-1}\otimes\cdots\otimes\boldsymbol{H}^{1} \tag{5}$$

in Ref. [4], where $N=G-1$, G is the number of cells and $\otimes$ represents the Kronecker product[18], thus $\boldsymbol{H}^{n}\in\mathbb{C}^{\sqrt[N]{M}\times\sqrt[N]{M}}$. Thus for the three-cell case as shown in Fig. 1, the channel coefficient matrix from the kth MS of the cell σ to the BS ψ is 2-level decomposable as:

$$\boldsymbol{H}_{\sigma k}^{\psi}=\boldsymbol{H}_{\sigma k}^{\psi,2}\otimes\boldsymbol{H}_{\sigma k}^{\psi,1},\ \sigma,\psi\in\{\alpha,\beta,\gamma\} \tag{6}$$

And in this case: $M=(\sqrt{K}+1)^2$, therefore,

$$\boldsymbol{H}_{\sigma k}^{\psi}\in\mathbb{C}^{(\sqrt{K}+1)^2\times(\sqrt{K}+1)^2} \tag{7}$$

and

$$\boldsymbol{H}_{\sigma k}^{\psi,1},\boldsymbol{H}_{\sigma k}^{\psi,2}\in\mathbb{C}^{(\sqrt{K}+1)\times(\sqrt{K}+1)} \tag{8}$$

Similarly, the precoder vector can be designed with 2-level decomposability as:

$$\mathbf{V}_{\sigma k}=\mathbf{V}_{\sigma k}^{2}\otimes\mathbf{V}_{\sigma k}^{1} \tag{9}$$

where

$$\mathbf{V}_{\sigma k}\in\mathbb{C}^{(\sqrt{K}+1)^2\times 1}\text{ and }\mathbf{V}_{\sigma k}^{2},\mathbf{V}_{\sigma k}^{1}\in\mathbb{C}^{(\sqrt{K}+1)\times 1}$$

The received signal at BS α can be reformulated as:

$$\mathbf{Y}_{\alpha}=\sum_{k=1}^{K}(\boldsymbol{H}_{\alpha k}^{\alpha,2}\otimes\boldsymbol{H}_{\alpha k}^{\alpha,1})(\mathbf{V}_{\alpha k}^{2}\otimes\mathbf{V}_{\alpha k}^{1})x_{\alpha k}+\sum_{k=1}^{K}(\boldsymbol{H}_{\beta k}^{\alpha,2}\otimes\boldsymbol{H}_{\beta k}^{\alpha,1})(\mathbf{V}_{\beta k}^{2}\otimes\mathbf{V}_{\beta k}^{1})x_{\beta k}+\sum_{k=1}^{K}(\boldsymbol{H}_{\gamma k}^{\alpha,2}\otimes\boldsymbol{H}_{\gamma k}^{\alpha,1})(\mathbf{V}_{\gamma k}^{2}\otimes\mathbf{V}_{\gamma k}^{1})x_{\gamma k} \tag{10}$$

Now the question is how to transform the interference alignment into a mathematical model. Thus we introduce the subspace interference covariance and build the cost function over precoder vectors.

First the interference covariance matrix $\boldsymbol{Q}_{\alpha}\in\mathbb{C}^{(\sqrt{K}+1)^2\times(\sqrt{K}+1)^2}$ at BS α can be expressed as:

$$\begin{aligned}\boldsymbol{Q}_{\alpha}=&\sum_{k=1}^{K}(\boldsymbol{H}_{\beta k}^{\alpha,2}\otimes\boldsymbol{H}_{\beta k}^{\alpha,1})(\mathbf{V}_{\beta k}^{2}\otimes\mathbf{V}_{\beta k}^{1})\cdot\\&(\mathbf{V}_{\beta k}^{2}\otimes\mathbf{V}_{\beta k}^{1})^{\dagger}(\boldsymbol{H}_{\beta k}^{\alpha,2}\otimes\boldsymbol{H}_{\beta k}^{\alpha,1})^{\dagger}+\\&\sum_{k=1}^{K}(\boldsymbol{H}_{\gamma k}^{\alpha,2}\otimes\boldsymbol{H}_{\gamma k}^{\alpha,1})(\mathbf{V}_{\gamma k}^{2}\otimes\mathbf{V}_{\gamma k}^{1})\cdot\\&(\mathbf{V}_{\gamma k}^{2}\otimes\mathbf{V}_{\gamma k}^{1})^{\dagger}(\boldsymbol{H}_{\gamma k}^{\alpha,2}\otimes\boldsymbol{H}_{\gamma k}^{\alpha,1})^{\dagger}\end{aligned} \tag{11}$$

From Eq. (11), we can see that the first item on the right hand side of the equation actually is the inter-cell interference from cell β and the second item is the inter-cell interference from cell γ. By exploring the property of Kronecker product:

$$(\mathbf{A}\otimes\boldsymbol{B})(\mathbf{C}\otimes\boldsymbol{D})=(\mathbf{AC})\otimes(\boldsymbol{BD}) \tag{12}$$

and

$$(\mathbf{A}\otimes\boldsymbol{B})^{\dagger}=\mathbf{A}^{\dagger}\otimes\boldsymbol{B}^{\dagger} \tag{13}$$

the inter-cell interference from cell β, i. e., the first item on the right hand side of the Eq. (11) can be reformulated as:

$$\begin{aligned}&\sum_{k=1}^{K}(\boldsymbol{H}_{\beta k}^{\alpha,2}\otimes\boldsymbol{H}_{\beta k}^{\alpha,1})(\mathbf{V}_{\beta k}^{2}\otimes\mathbf{V}_{\beta k}^{1})\cdot\\&(\mathbf{V}_{\beta k}^{2}\otimes\mathbf{V}_{\beta k}^{1})^{\dagger}(\boldsymbol{H}_{\beta k}^{\alpha,2}\otimes\boldsymbol{H}_{\beta k}^{\alpha,1})^{\dagger}=\\&\sum_{k=1}^{K}\{(\boldsymbol{H}_{\beta k}^{\alpha,2}\mathbf{V}_{\beta k}^{2})\otimes(\boldsymbol{H}_{\beta k}^{\alpha,1}\mathbf{V}_{\beta k}^{1})\}\cdot\\&\{(\mathbf{V}_{\beta k}^{2\dagger}\boldsymbol{H}_{\beta k}^{\alpha,2\dagger})\otimes(\mathbf{V}_{\beta k}^{1\dagger}\boldsymbol{H}_{\beta k}^{\alpha,1\dagger})\}=\\&\sum_{k=1}^{K}\{(\boldsymbol{H}_{\beta k}^{\alpha,2}\mathbf{V}_{\beta k}^{2}\mathbf{V}_{\beta k}^{2\dagger}\boldsymbol{H}_{\beta k}^{\alpha,2\dagger})\otimes(\boldsymbol{H}_{\beta k}^{\alpha,1}\mathbf{V}_{\beta k}^{1}\mathbf{V}_{\beta k}^{1\dagger}\boldsymbol{H}_{\beta k}^{\alpha,1\dagger})=\\&\sum_{k=1}^{K}\boldsymbol{Q}_{\beta k}^{\alpha,2}\otimes\boldsymbol{Q}_{\beta k}^{\alpha,1}\end{aligned} \tag{14}$$

Similarly, reformulation is employed for the inter-cell interference from cell γ. Finally Eq. (11) is reformed as:

$$\boldsymbol{Q}^{\alpha}=\sum_{k=1}^{K}\boldsymbol{Q}_{\beta k}^{\alpha,2}\otimes\boldsymbol{Q}_{\beta k}^{\alpha,1}+\sum_{k=1}^{K}\boldsymbol{Q}_{\gamma k}^{\alpha,2}\otimes\boldsymbol{Q}_{\gamma k}^{\alpha,1} \tag{15}$$

It can be obtained that:

$$\boldsymbol{Q}^{\alpha}=\boldsymbol{Q}_{\beta}^{\alpha,2}\otimes\boldsymbol{Q}_{\beta}^{\alpha,1}+\boldsymbol{Q}_{\gamma}^{\alpha,2}\otimes\boldsymbol{Q}_{\gamma}^{\alpha,1} \tag{16}$$

where

$$\boldsymbol{Q}_{\beta}^{\alpha,1},\boldsymbol{Q}_{\beta}^{\alpha,2},\boldsymbol{Q}_{\gamma}^{\alpha,1},\boldsymbol{Q}_{\gamma}^{\alpha,2}\in\mathbb{C}^{(\sqrt{K}+1)\times(\sqrt{K}+1)}$$

are the subspace interference covariance matrices, and

$$\boldsymbol{Q}_{\beta}^{\alpha,i}=\sum_{k=1}^{K}\boldsymbol{H}_{\beta k}^{\alpha,i}\boldsymbol{V}_{\beta k}^{i}\boldsymbol{V}_{\beta k}^{i\dagger}\boldsymbol{H}_{\beta k}^{\alpha,i\dagger} \tag{17}$$

$$\boldsymbol{Q}_{\gamma}^{\alpha,i}=\sum_{k=1}^{K}\boldsymbol{H}_{\gamma k}^{\alpha,i}\boldsymbol{V}_{\gamma k}^{i}\boldsymbol{V}_{\gamma k}^{i\dagger}\boldsymbol{H}_{\gamma k}^{\alpha,i\dagger} \tag{18}$$

where $i\in\{1,2\}$. Similarly, the interference covariance matrices $\boldsymbol{Q}^{\beta}$ and $\boldsymbol{Q}^{\gamma}$ at BS β and BS γ can also be represented as the sum of Kronecker product of corresponding subspace interference covariance.

$$\boldsymbol{Q}^{\beta}=\boldsymbol{Q}_{\alpha}^{\beta,2}\otimes\boldsymbol{Q}_{\alpha}^{\beta,1}+\boldsymbol{Q}_{\gamma}^{\beta,2}\otimes\boldsymbol{Q}_{\gamma}^{\beta,1} \tag{19}$$

$$\boldsymbol{Q}^{\gamma}=\boldsymbol{Q}_{\beta}^{\gamma,2}\otimes\boldsymbol{Q}_{\beta}^{\gamma,1}+\boldsymbol{Q}_{\alpha}^{\gamma,2}\otimes\boldsymbol{Q}_{\alpha}^{\gamma,1} \tag{20}$$

From Eqs. (16)～(20), it can be acquired that we separate subspace 1 and subspace 2 completely by its own subspace interference covariance. As known in Ref. [8], the quality of alignment is measured by the interference power remaining in the intended signal subspace at each receiver. Therefore, interference alignment can be achieved by iteratively reducing the remaining interference to zero. From Ref. [9], it can be obtained that the eigenvectors of the interference covariance matrices span the dimensions of interference subspace and their corresponding eigenvalues indicate the power of interference along that dimension. Take 3IMAC for example, as shown in Fig. 1, at BS α, we must both minimize the sum of $\sqrt{K}$-smallest eigenvalues of $\boldsymbol{Q}_{\beta}^{\alpha,1}$ and that of $\boldsymbol{Q}_{\gamma}^{\alpha,2}$ to force the inter-cell interference overlapping in one dimension at subspace 1 and subspace 2, respectively; meanwhile, similarly at BS β (and BS γ) the corresponding sum of $\sqrt{K}$-smallest eigenvalues of subspace interference covariances $\boldsymbol{Q}_{\gamma}^{\beta,1}$ and $\boldsymbol{Q}_{\alpha}^{\beta,2}$ ($\boldsymbol{Q}_{\alpha}^{\gamma,1}$ and $\boldsymbol{Q}_{\alpha}^{\gamma,2}$) are also minimized to zero. This process can be described as:

$$\min f=\sum_{\substack{\sigma,\psi\in\{\alpha,\beta,\gamma\}\\ \sigma\neq\psi}}\sum_{j=1,2}\text{Sum\_eigvalue}(\boldsymbol{Q}_{\psi}^{\sigma,j})_{\sqrt{K}} \tag{21}$$

where

$$\boldsymbol{Q}_{\sigma}^{\psi,g}=\sum_{k=1}^{K}\boldsymbol{H}_{\sigma k}^{\psi,i}\boldsymbol{V}_{\sigma k}^{i}\boldsymbol{V}_{\sigma k}^{i\dagger}\boldsymbol{H}_{\sigma k}^{\psi,i\dagger} \tag{22}$$

and here we define $\text{Sum\_eigvalue}(\boldsymbol{Q}_{\sigma}^{\psi,g})_{\sqrt{K}}$ as the sum of the $\sqrt{K}$ smallest eigenvalues of $\boldsymbol{Q}_{\sigma}^{\psi,g}$. Thus we can create K-dimensional interference-free subspace and achieve subspace alignment.

Now we generalize our idea for G-cell ($G\geqslant 3$) case subspace interference alignment. In this case the dimension size $M=(\sqrt[G-1]{K}+1)^{G-1}$, and the channel matrix $\boldsymbol{H}_{ik}^{j}\in\mathbb{C}^{M\times M}$ from the kth MS in the cell σ to the BS ψ can be $G-1$ level decomposed as:

$$\boldsymbol{H}_{\sigma k}^{j}=\bigotimes_{g=1}^{G-1}\boldsymbol{H}_{\sigma k}^{\psi,g}=\boldsymbol{H}_{\sigma k}^{\psi,G-1}\otimes\boldsymbol{H}_{\psi k}^{\psi,G-2}\otimes\cdots\cdots\otimes\boldsymbol{H}_{\sigma k}^{\psi,1} \tag{23}$$

where

$$\sigma,\psi\in\{1,2,\cdots,G\} \tag{24}$$

and

$$\boldsymbol{H}_{\sigma k}^{\psi,g}\in\mathbb{C}^{\sqrt[G-1]{M}\times\sqrt[G-1]{M}} \tag{25}$$

Similarly, we design the beaforming precoder of the kth MS in the cell σ with G-level decomposability as:

$$\boldsymbol{V}_{\sigma k}=\bigotimes_{g=1}^{G-1}\boldsymbol{V}_{\sigma k}^{g}=\boldsymbol{V}_{\sigma k}^{G-1}\otimes\boldsymbol{V}_{\sigma k}^{G-2}\cdots\otimes\boldsymbol{V}_{\sigma k}^{1} \tag{26}$$

where

$$\boldsymbol{V}_{\sigma k}^{g}\in\mathbb{C}^{\sqrt[G-1]{M}\times 1} \tag{27}$$

Therefore, as previously stated, we can define the cost function over the set of precoder vectors $\boldsymbol{V}_{\sigma k}^{g}$ by

$$\left.\begin{aligned}&\min f=\sum_{\substack{\sigma,\psi=1\\ \sigma\neq\psi}}^{G}\sum_{g=1}^{G-1}\text{Sum\_eigvalue}(\boldsymbol{Q}_{\sigma}^{\psi,g})_{\sqrt[G-1]{K}}\\&\text{subject to }\boldsymbol{V}_{\sigma k}^{g\dagger}\boldsymbol{V}_{\sigma k}^{g}=1\end{aligned}\right\} \tag{28}$$

and because $\boldsymbol{Q}_{\sigma}^{\psi,g}$ is a Hermitian matrix, all its eigenvalues are real. Finally, the cost function $f(\boldsymbol{V}_{\sigma k}^{g})$, $f:\mathbb{C}^{n\times p}\to\mathbb{R}^{+}$ is built. It is easy to obtain that in fact our cost function is the normalized remnant interference.

3 The steepest descent algorithm on Grassmann manifold

Since our cost function: $f:\mathbb{C}^{n\times p}\to\mathbb{R}^{+}$ is differentiable[19], intuitively the steepest descent (SD) method can be employed to make the cost function converge to a local optimal point

efficiently. However, as discussed before, the traditional optimization methods, including the classical SD algorithm, work in high-dimensional complex space. They will suffer from high computational complexity, slow convergence and large residual interference.

Thus we introduce optimization on Grassmann manifold to reduce the dimensions of space while achieving total computational complexity and faster convergence. A manifold is a subspace which is embedded in Euclidean space (The broadest common definition of manifold is a topological space locally homeomorphic to a topological vector space). It can be informally defined as a subset of Euclidean space which is locally the graph of a smooth function[20].

Consequently, different from transitional SD method, we should notice some problems for optimization on manifolds. First, in order to define algorithms on manifolds, these operations above must be translated into the language of differential geometry. Second, once the test point moves along the steepest descent direction for certain distance, it must be retracted back to the manifold. Third, we should choose a simple but efficient step size rule for each iteration. Therefore, after reformulating the constrained optimization problem on manifold to a unconstrained one, we will introduce definitions about project operation and tangent space for retraction and gradient respectively; meanwhile we employ modified Armijo step rule for each iteration.

The underlying symmetry property can be exploited to reformulate the original problem as a non-degenerate optimization problem on manifolds associated with the original matrix representation. Thus the constraint condition $\mathbf{V}_{dk}^{g\dagger}\mathbf{V}_{dk}^{g}=1$ of our cost function (28) seems to inspire us to solve the problem of the complex Stiefel manifold. The complex Stiefel manifold[18] can be defined as:

$$\mathrm{St}(n,p)=\{\boldsymbol{X}\in\mathbb{C}^{n\times p}:\boldsymbol{X}^{\dagger}\boldsymbol{X}=\boldsymbol{I}\} \tag{29}$$

$\mathrm{St}(n,p)$ is naturally embeded in $\mathbb{C}^{n\times p}$ and inherits the usual topology of $\mathbb{C}^{n\times p}$. It is a compact manifold and from Proposition 3.3.3 in Ref.[20], we can obtain:

$$\dim(\mathrm{St}(n,p))=np-\frac{1}{2}p(p+1) \tag{30}$$

and remind the fact that the traditional optimization methods used by Refs.[8-14] works in the multi-dimensional space $\mathbb{C}^{n\times p}$ with the dimensions:

$$\dim(\mathbb{C}^{n\times p})=np \tag{31}$$

From Eqs.(30) to (31), it can be obtained that if we reformulate the original problem of the Stiefel manifold, the dimensions of space decreases from $n\times p$ to $np-\frac{1}{2}p(p+1)$. The detailed procedure can be found in Ref.[21].

Although such dimension-dissension can be observed clearly, we still intend to reduce the dimensions of the space which the optimization algorithm works in. Notice that our cost function $f(\mathbf{V})$ satisfies $f(\mathbf{VU})=f(\mathbf{V})$ for any unitary matrix $\mathbf{U}$. Because

$$\boldsymbol{Q}_{\sigma}^{\psi,g}(\mathbf{V}_{dk}^{g}\mathbf{U})=\sum_{k=1}^{K}\boldsymbol{H}_{dk}^{\psi,g}\mathbf{V}_{dk}^{g}\mathbf{U}\mathbf{U}^{\dagger}\mathbf{V}_{dk}^{g\dagger}\boldsymbol{H}_{dk}^{\psi,g\dagger}=\sum_{k=1}^{K}\boldsymbol{H}_{dk}^{\psi,g}\mathbf{V}_{dk}^{g}\boldsymbol{I}\mathbf{V}_{dk}^{g\dagger}\boldsymbol{H}_{dk}^{\psi,g\dagger}=\boldsymbol{Q}_{\sigma}^{\psi,g}(\mathbf{V}_{dk}^{g}) \tag{32}$$

which means that multiplying unitary matrix $\mathbf{U}$ does not change the eigenvalues of the interference covariance matrices. Thus our cost function f should be considered on the Grassmann manifold instead of the Stiefel manifold. The reason is that the Grassmann manifold treats $\mathbf{V}$ and $\mathbf{VU}$ as equivalent points, thus leading to a further dimension descension of the optimization problem.

The complex Grassmann manifold $Gr(n,p)$ is the set of all p-dimensional complex subspaces of $\mathbb{C}^{n\times p}$. From Eq.(30), it can be obtained that:

$$\dim(Gr(n,p))=\dim(St(n,p))-\dim(St(p,p))=p(n-p) \tag{33}$$

From Eqs. (31) to (33), the further dimension descent can be observed clearly which is an advantage of optimization on Grassmann manifold. This is because Grassmann manifold can

be thought of as a quotient space of the Stiefel manifold. That is to say, if $\lfloor \boldsymbol{X} \rfloor$ represents the subspace spanned by the columns of $\boldsymbol{X}$, then $\boldsymbol{X} \in St(n, p)$ means $\lfloor \boldsymbol{X} \rfloor \in Gr(n, p)$. Therefore, there is a one-to-one mapping between equivalence classes of $St(n, p)$ and points on the Grassmann manifold $Gr(n, p)$.

As previously stated, for retracting the test point back into the manifold, we must define the project operation. Let $\boldsymbol{X} \in St(n, p)$ be a rank p matrix. The projection operator $\pi: \mathbb{C}^{n\times p} \to Gr(n, p)$ is defined to be

$$\pi(\boldsymbol{Y}) = \lfloor \arg \min_{\boldsymbol{X}\in St(n,p)} \| \boldsymbol{Y} - \boldsymbol{X} \|^2 \rfloor \tag{34}$$

From Eq. (34), it can be acquired that the projection of a random rank p matrix $\boldsymbol{Y}$ onto the Grassmannn manifold can be defined as the subspace spanned by the point on the Stiefel manifold closest to $\boldsymbol{Y}$ in the Euclidean norm. Besides, if the QR decomposition of $\boldsymbol{Y}$ is $\boldsymbol{Y} = \boldsymbol{QR}$,

$$\pi(\boldsymbol{Y}) = \lfloor \boldsymbol{Q}\boldsymbol{I}_{n\times p} \rfloor \tag{35}$$

The proof of Eq. (35) can be found in Ref. [22]. From Eq. (35), it can be obtained that, if the $\boldsymbol{QR}$ decomposition of $\boldsymbol{Y}$ is $\boldsymbol{Y} = \boldsymbol{QR}$, then $\pi(\boldsymbol{Y})$ is the subspace spanned by the first p columns of the matrix $\boldsymbol{Q}$.

Consider $\boldsymbol{X} \in St(n, p)$ which implies $\lfloor \boldsymbol{X} \rfloor \in Gr(n, p)$ and its disturbing point $\pi(\boldsymbol{X} + \varepsilon \boldsymbol{Y}) \in Gr(n, p)$ for certain directions matrix $\boldsymbol{Y} \in \mathbb{C}^{n\times p}$ and scalar $\varepsilon \in \mathbb{R}$. If $\boldsymbol{Y}$ satisfies $f(\pi(\boldsymbol{X}+\varepsilon\boldsymbol{Y})) = f(\boldsymbol{X}) + O(\varepsilon^2)$ which means certain directions $\boldsymbol{Y}$ do not cause $\pi(\boldsymbol{X} + \varepsilon\boldsymbol{Y})$ to move away from $\boldsymbol{X}$ as ε increases. The collection of such directions $\boldsymbol{Y}$ is called the normal space at $\boldsymbol{X}$ of $Gr(n, p)$[20]. The tangent space $T_{\lfloor \boldsymbol{X} \rfloor}(n, p)$ is defined to be the orthogonal complement of the normal space. The mathematical expression of the tangent space $T_{\lfloor \boldsymbol{X} \rfloor}(n, p)$ at $\lfloor \boldsymbol{X} \rfloor \in Gr(n, p)$ is defined by:

$$T_{\lfloor \boldsymbol{X} \rfloor}(n, p) = \{ \boldsymbol{Z} \in \mathbb{C}^{n\times p} : \boldsymbol{Z} = \boldsymbol{X}_\perp \boldsymbol{B}, \boldsymbol{B} \in \mathbb{C}^{(n-p)\times p} \} \tag{36}$$

where $\boldsymbol{X}_\perp \in \mathbb{C}^{n\times(n-p)}$ is defined to be any matrix satisfying $[\boldsymbol{X} \quad \boldsymbol{X}_\perp]^\dagger [\boldsymbol{X} \quad \boldsymbol{X}_\perp] = \boldsymbol{I}$ and is the complement of $\boldsymbol{X} \in St(n, p)$. Also from Ref. [22], it can be obtained that the tangent space of Grassmann manifold involves the gradient of manifold.

Obviously, the steepest descent algorithm needs the computation of the gradient. However the gradient is only defined after $T_{\lfloor \boldsymbol{X} \rfloor}(n, p)$ is given an inner product

$$\langle \boldsymbol{Z}_1, \boldsymbol{Z}_2 \rangle = \mathcal{R}\{\mathrm{tr}(\boldsymbol{Z}_2^\dagger \boldsymbol{Z}_1)\},$$
$$\boldsymbol{Z}_1, \boldsymbol{Z}_2 \in T_{\lfloor \boldsymbol{X} \rfloor}(n, p), \boldsymbol{X} \in St(n, p) \tag{37}$$

whose derivation can be found in Ref. [16]. Therefore, under the defined inner product, the steepest descent direction[22] of the cost function $f(\boldsymbol{X})$ at the point $\boldsymbol{X} \in Gr(n, p)$ is:

$$\boldsymbol{Z} = -(\boldsymbol{I} - \boldsymbol{X}\boldsymbol{X}^\dagger)\boldsymbol{D}_X \tag{38}$$

where $\boldsymbol{D}_X$ is the derivative of $f(\boldsymbol{X})$.

Considering our cost function $f(\boldsymbol{V})$ is $f: \mathbb{C}^{n\times p} \to \mathbb{R}^+$, we can get the first order derivative by using two Jacobian matrix blocks:

$$\begin{aligned} \mathrm{d}f = &\begin{bmatrix} \boldsymbol{RD}_{\sigma 1}^1, \boldsymbol{RD}_{\sigma 2}^1, \cdots \boldsymbol{RD}_{\sigma \mathrm{K}}^1 \\ \boldsymbol{RD}_{\sigma 1}^2, \boldsymbol{RD}_{\sigma 2}^2, \cdots \boldsymbol{RD}_{\sigma \mathrm{K}}^2 \\ \vdots \\ \boldsymbol{RD}_{\sigma 1}^{G-1}, \boldsymbol{RD}_{\sigma 2}^{G-1}, \cdots \boldsymbol{RD}_{\sigma \mathrm{K}}^{G-1} \end{bmatrix} \cdot \\ &\begin{bmatrix} \boldsymbol{d}\mathcal{R}\{\mathbf{V}_{\sigma 1}^1\}, \boldsymbol{d}\mathcal{R}\{\mathbf{V}_{\sigma 1}^2\}, \cdots \boldsymbol{d}\mathcal{R}\{\mathbf{V}_{\sigma 1}^{G-1}\} \\ \boldsymbol{d}\mathcal{R}\{\mathbf{V}_{\sigma 2}^1\}, \boldsymbol{d}\mathcal{R}\{\mathbf{V}_{\sigma 2}^2\}, \cdots \boldsymbol{d}\mathcal{R}\{\mathbf{V}_{\sigma 2}^{G-1}\} \\ \vdots \\ \boldsymbol{d}\mathcal{R}\{\mathbf{V}_{\sigma \mathrm{K}}^1\}, \boldsymbol{d}\mathcal{R}\{\mathbf{V}_{\sigma \mathrm{K}}^2\}, \cdots \boldsymbol{d}\mathcal{R}\{\mathbf{V}_{\sigma \mathrm{K}}^{G-1}\} \end{bmatrix} + \\ &\begin{bmatrix} \boldsymbol{ID}_{\sigma 1}^1, \boldsymbol{ID}_{\sigma 2}^1, \cdots \boldsymbol{ID}_{\sigma \mathrm{K}}^1 \\ \boldsymbol{ID}_{\sigma 1}^2, \boldsymbol{ID}_{\sigma 2}^2, \cdots \boldsymbol{ID}_{\sigma \mathrm{K}}^2 \\ \vdots \\ \boldsymbol{ID}_{\sigma 1}^{G-1}, \boldsymbol{ID}_{\sigma 2}^{G-1}, \cdots \boldsymbol{ID}_{\sigma \mathrm{K}}^{G-1} \end{bmatrix} \cdot \\ &\begin{bmatrix} \boldsymbol{d}\mathcal{I}\{\mathbf{V}_{\sigma 1}^1\}, \boldsymbol{d}\mathcal{I}\{\mathbf{V}_{\sigma 1}^2\}, \cdots \boldsymbol{d}\mathcal{I}\{\mathbf{V}_{\sigma 1}^{G-1}\} \\ \boldsymbol{d}\mathcal{I}\{\mathbf{V}_{\sigma 2}^1\}, \boldsymbol{d}\mathcal{I}\{\mathbf{V}_{\sigma 2}^2\}, \cdots \boldsymbol{d}\mathcal{I}\{\mathbf{V}_{\sigma 2}^{G-1}\} \\ \vdots \\ \boldsymbol{d}\mathcal{I}\{\mathbf{V}_{\sigma \mathrm{K}}^1\}, \boldsymbol{d}\mathcal{I}\{\mathbf{V}_{\sigma \mathrm{K}}^2\}, \cdots \boldsymbol{d}\mathcal{I}\{\mathbf{V}_{\sigma \mathrm{K}}^{G-1}\} \end{bmatrix} \end{aligned} \tag{39}$$

$\boldsymbol{RD}_{\sigma k}^g$ and $\boldsymbol{ID}_{\sigma k}^g$ are the $1 \times \sqrt[G-1]{M}$ Jacobian vectors which denote the partial differential relation of the cost function over the real and imaginary parts of $\mathbf{V}_{\psi k}$ respectively. The detail of mathematical derivations can be found in Refs. [14, 18]. Thus, the derivative of f over $\mathbf{V}_{\sigma k}^g$ is given by

$$\boldsymbol{D}_{\sigma k}^g = (\boldsymbol{RD}_{\sigma k}^g + j\boldsymbol{ID}_{\sigma k}^g)^{\mathrm{T}} \tag{40}$$

Once the formulation of steepest descent

direction $\mathbf{Z}$ on Grassmann manifold is defined, it is necessary to choose a suitable positive step size β for each iteration. The Armijo step size rule[23] states that β should be chosen to satisfy the following inequalities:

$$f(\mathbf{V}) - f(\mathbf{V}+\beta\mathbf{Z}) \geqslant \frac{1}{2}\beta\langle \mathbf{Z},\mathbf{Z}\rangle \qquad (41)$$

$$f(\mathbf{V}) - f(\mathbf{V}+2\beta\mathbf{Z}) < \beta\langle \mathbf{Z},\mathbf{Z}\rangle \qquad (42)$$

Rule (41) guarantees that the step $\beta\mathbf{Z}$ will expressively decrease the cost function, whereas function (42) undertakes that the step $2\beta\mathbf{Z}$ would not be a better choice. A direct procedure for acquiring a suitable β is to keep on doubling β until function (42) no longer holds and then halving β until it satisfies function (41). It can be proved that such β can always be found[24].

Consolidating all the ideas stated above, the proposed SD algorithm on complex Grassmann manifold is presented in Algorithm 3.1.

Algorithm 3.1 The steepest descent algorithm on complex Grassmann manifold

Start with arbitrary precoder matrices $\mathbf{V}_{\sigma 1}^{g},\cdots,\mathbf{V}_{\sigma K}^{g}$, and begin iteration.

for $\sigma=1,2,\cdots G$

for $g=1,2,\cdots G-1$

for $k=1\cdots K$

Step 1 Compute the Jacobian matrix $\boldsymbol{RD}_{\sigma k}^{g}$ and $\boldsymbol{ID}_{\sigma k}^{g}$

Step 2 Then get the derivative of f:

$$\mathbf{D}_{\sigma k}^{g} = (\boldsymbol{RD}_{\sigma k}^{g} + j\boldsymbol{ID}_{\sigma k}^{g})^{\mathrm{T}}$$

Step 3 Get the steepest descent direction

$$\mathbf{Z}_{\sigma k}^{g} = -(\boldsymbol{I}-\mathbf{V}_{\sigma k}^{g}\mathbf{V}_{\sigma k}^{g\dagger})\mathbf{D}_{\sigma k}^{g}$$

Step 4 Compute $\mathbf{A}_{\sigma k}^{g}=\pi(\mathbf{V}_{\sigma k}^{g}+2\beta_{\sigma k}^{g}\mathbf{Z}_{\sigma k}^{g})$, if $f(\mathbf{V}_{\sigma 1}^{g},\cdots,\mathbf{V}_{\sigma K}^{g}) - f(\mathbf{V}_{\sigma 1}^{g},\cdots,\mathbf{V}_{\sigma(k-1)}^{g},\mathbf{A}_{\sigma k}^{g},\cdots\mathbf{V}_{\sigma K}^{g}) \geqslant \beta_{\sigma k}^{g}\,\mathrm{tr}(\mathbf{Z}_{\sigma k}^{g\dagger}\mathbf{Z}_{\sigma k}^{g})$, then set $\beta_{\sigma k}^{g} := 2\beta_{\sigma k}^{g}$, and repeat Step 4.

Step 5 Compute $\mathbf{B}_{\sigma k}^{g}=\pi(\mathbf{V}_{\sigma k}^{g}+\beta_{k}\mathbf{Z}_{\sigma k}^{g})$, if $f(\mathbf{V}_{\sigma 1}^{g},\cdots,\mathbf{V}_{\sigma K}^{g}) - f(\mathbf{V}_{\sigma 1}^{g},\cdots,\mathbf{V}_{\sigma(k-1)}^{g},\mathbf{B}_{\sigma k}^{g},\cdots\mathbf{V}_{\sigma K}^{g}) < \frac{1}{2}\beta_{\sigma k}^{g}\,\mathrm{tr}(\mathbf{Z}_{\sigma k}^{g\dagger}\mathbf{Z}_{\sigma k}^{g})$, then set $\beta_{\sigma k}^{g} := \frac{1}{2}\beta_{\sigma k}^{g}$, and repeat Step 5.

Step 6 $\mathbf{V}_{\sigma k}^{g}=\pi(\mathbf{V}_{\sigma k}^{g}+\beta_{\sigma k}^{g}\mathbf{Z}_{\sigma k}^{g})$

Step 7 Continue till the cost function f is sufficiently small.

Inspired by Ref. [22], the structure of the proposed algorithm is intuitive. Here some explanations are presented. In Steps 4 and 5, the Armijo step rule[24] is performed to find a proper convergence step length $\beta_{\sigma k}^{g}$. From Eq. (37) and Eq. (38), it can be easily obtained that the inner product needed for the Armijo step rule is

$$\langle \mathbf{Z}_{\sigma k}^{g},\mathbf{Z}_{\sigma k}^{g}\rangle = \mathrm{tr}(\mathbf{Z}_{\sigma k}^{g\dagger}\mathbf{Z}_{\sigma k}^{g}) \qquad (43)$$

which is used in Steps 4 and 5; and the steepest descent on Grassmann manifold of our cost function is

$$\mathbf{Z}_{\sigma k}^{g} = -(\boldsymbol{I}-\mathbf{V}_{\sigma k}^{g}\mathbf{V}_{\sigma k}^{g\dagger})\mathbf{D}_{\sigma k}^{g} \qquad (44)$$

which was used in Step 3. Noticing that the project operation $\pi(\cdot)$ in Step 6 (Steps 4, 5) guarantees the newly computed solution $\mathbf{V}_{\sigma k}^{g}$ (or $\mathbf{A}_{\sigma k}^{g}$, $\boldsymbol{B}_{\sigma k}^{g}$) after iteration still satisfies $\mathbf{V}_{\sigma k}^{g}\in Gr(M,1)$. Using $\boldsymbol{QR}$ decomposition, we can easily compute the project operation.

Discussion:

(Ⅰ) The inner product and the gradient direction are defined in different topologies in Ref. [14]. However it is considered to be inappropriate because the gradient is defined only after the inner product is given. In other words, the inner product and the gradient direction must be defined in the same topology. Our proposed algorithm avoids the topology flaw in Ref. [14].

(Ⅱ) Some optimization methods on manifolds such as algorithms in Refs. [15-17] are performed by moving the descent step along the geodesic of the constrained surface within each iteration. There are two major disadvantages of these methods. One is the redundant computational cost for calculating the path of a geodesic[22]. Another disadvantage is that rules for the linear steps, such as Armijo step rule, can not be employed to make iteration more efficient. Different from these methods, in this paper we locally parameterize the manifold by Euclidean projection from the tangent space onto the manifold instead of moving along a geodesic, to achieve a modest reduction in the computational complexity of the algorithms.

(Ⅲ) To sum up, compared with the transitional optimization methods which work in $\mathbb{C}^{n\times p}$, the proposed SD algorithm on Grassmann manifold obviously has

$$\frac{\dim(Gr(n,p))}{\dim(\mathbb{C}^{n\times p})}=\frac{p(n-p)}{np} \tag{45}$$

In our subspace interference alignment system model,

$$n=M=(\sqrt[G-1]{K}+1)^{G-1} \tag{46}$$

and $p=K$. Thus we can get:

$$\frac{\dim(Gr(M,K))}{\dim(\mathbb{C}^{M\times K})}=\frac{K[(\sqrt[G-1]{K}+1)^{G-1}-K]}{K(\sqrt[G-1]{K}+1)^{G-1}} \tag{47}$$

and if K is large enough, then

$$\frac{\dim(Gr(M,K))}{\dim(\mathbb{C}^{M\times K})}\approx\frac{1}{K} \tag{48}$$

which is clear evidence for dimension-descension.

4　Numerical results and discussion

For satisfying feasibility and simple computation, firstly we simulate the three-cell case where four MSs in each cell ($G=3$, $K=4$). And each MS sends one symbol message to its corresponding BS. Thus the dimensions of desired signal space per cell is $M=9$, and the DoF per cell is $\frac{4}{9}$. We simulated the SD algorithm on Grassmann manifold for IA through 100 randomly generated channel coefficients and initial precoder matrices. According to the numerical feasibility criterion of interference alignment in Ref. [9], the cost function must fall below 10^{-4}. As shown in Fig. 2, each curve represents an individual simulation realization and all results converge after 20 or more iterations.

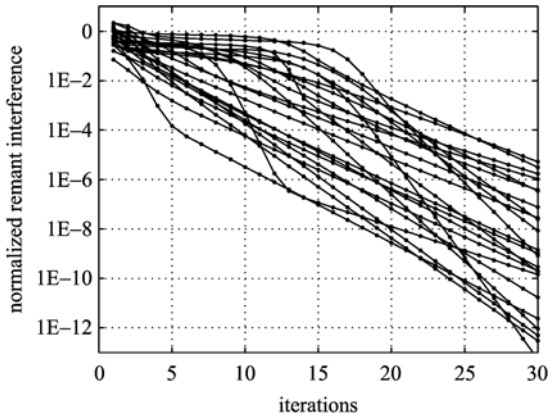

Fig. 2　The cost function (normalized remnant interference) of SD algorithm on Grassmann manifold

Furthermore, in order to compare the convergence performance, our proposed SD algorithm on Grassmann manifold for IA and the algorithm in Refs. [8-9,14] are executed under the same scenario including randomly generated channel coefficients, initial precoder matrices and convergence step length. The average values are shown in Fig. 3. It can be observed that the SD algorithm on Grassmann manifold has better convergence performance. This is attributed to the fact that the proposed algorithm reformulates the constrained optimization problem to an unconstrained one on manifold with better numerical properties. Note that the algorithm in Refs. [8-9] and [14] which employ traditional methods work in the dimension of np, while our proposed SD algorithm on Grassmann manifold works in the dimensions of $p(n-p)$. And by setting $K=4$ and $G=3$ and then taking them into (47), it can be derived that $\frac{\dim(Gr(M,d))}{\dim(\mathbb{C}^{M\times d})}=\frac{5}{9}$. Obviously, the dimensions reduction will make the proposed algorithm converge faster. Moreover, from Refs. [18,22] and [25], it can be obtained that the asymptotic computational complexity per iteration of our proposed algorithm is $O(M^3)$ which is the same as the algorithms in Refs. [8-9] and [14]. Since our method needs less iterations to converge, the total computational complexity is lower than that of previous methods. In all, it can be obtained that our algorithm has better

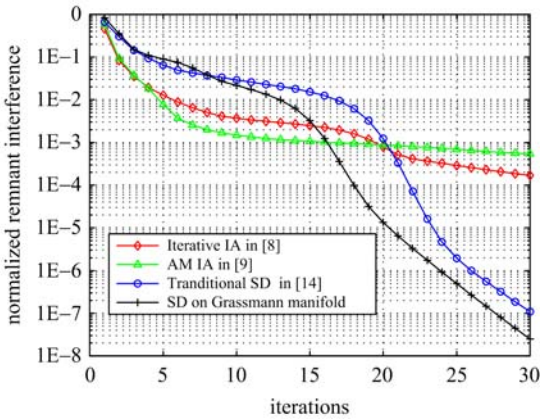

Fig. 3　Convergence performance

convergence performance and lower total computational complexity.

The proof of convergence of the proposed algorithm is intuitive. Our cost function is non-negative whose low bound is zero and monotonically decreases within each iteration. Therefore it must converge to a local optimum solution which is very close to zero. However, there is no guarantee that our cost function is convex[8]. Thus finding a global optimum is a goal in our future work.

We also do some simulations by using more sophisticated algorithm, such as Newton-type method, to achieve quadratic convergence. Yet, except for the increased computational complexity, the Newton method will converge to the closet critical point[22]. Thus the Newton method coupled with the steepest descent algorithm will be investigated in our future work, too.

Finally, we compare the system sum-rate per cell of the proposed algorithms. Fig. 4 shows the scenario of 3 cells and 4 MSs per cell. And Fig. 5 shows the scenario of 4 cells and 8 MSs per cell. Both simulation results demonstrate that the SD algorithm on Grassmann manifold outperforms the other algorithms. More importantly, in the two scenarios it can be easily obtained that the DoF per cell of the proposed algorithm at high SNR nearly approaches 4/9 and 8/27 separately, which are the theoretical maximum values. Therefore, the subspace interference alignment is successfully

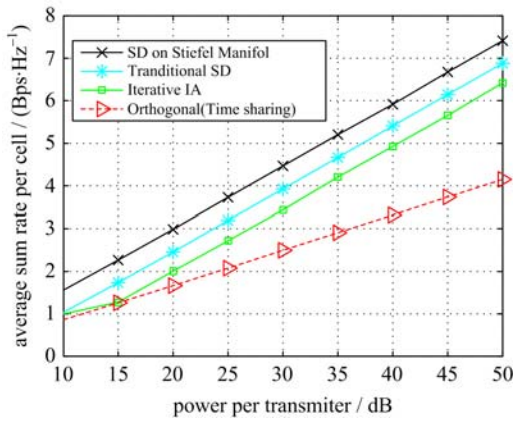

Fig. 4 3 cells and 4 MSs per cell ($G=3$, $K=4$ **per cell**)

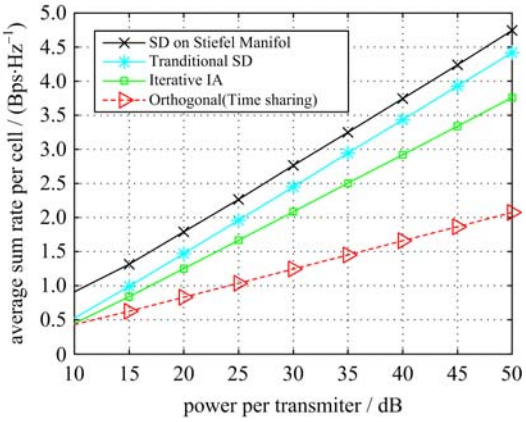

Fig. 5 4 cells and 8 MSs per cell ($G=4$, $K=8$ **per cell**)

achieved.

Two reasons leading to the fact that the algorithms on Grassmann manifold obtain higher system capacity are presented below:

(Ⅰ) It is noticed that our cost function actually is the interference power spilled from the interference space to the desired signal space. The SD algorithms on manifolds will have less remnant interference in the desired signal space within the same iteration times. Therefore, the SD algorithms on manifolds will get higher SINR[8]:

$$\mathrm{SINR}=\frac{\text{signal power}}{\text{noise}+\text{remnant interference}} \tag{49}$$

which leads to high capacity.

(Ⅱ) At each receiver, the zero forcing filter is adopted. It will project the desired signal power and the remnant interference onto the subspace which is orthogonal with the subspace spanned by the interference. After performing the SD algorithms on Grassmann manifold, it is observed that in the Euclidean norm distance, the subspace spanned by desired signal is closer to the orthogonal complement of the interference subspace. Therefore, our proposed algorithm finally gets the same remnant interference as the traditional optimization methods results. The algorithms on manifolds will suffer less from power lose during the projection operated by zero forcing filter, hence achieving higher system capacity.

We notice that better throughput performance

of our method may be attained by applying power water-filling in the equivalent non-interfering MIMO channels or by being combined with other interference suppression technologies. Nevertheless, these methods for increasing throughputs can be performed as the second step after the interference alignment is achieved[15]. Thus in this paper, we only need to concentrate on the first step to find the perfect solutions of subspace interference alignment.

Finally, we discuss the difference between our precoder design method and the methods[8-13] based on a joint design of precoder and receiving filter at both sides of transceivers. By utilizing channel reciprocity, the joint design methods achieve interference alignment by alternating between the forward and reverse links to achieve interference alignment in a distributed way. The applicability of their proposed algorithms are limited only to TDD systems due to the assumption of channel reciprocity. Moreover, this alternation needs synchronization at each node, which may introduce too much overhead when the channel varies quickly. As previously stated, by restricting the optimization only at the transmitters' side, our method achieves interference alignment with precoder design only. Although our method may need the interference link channel information, it will alleviate the redundant overhead generated by alternation between the up and down links. Furthermore, by relaxing the assumption of channel reciprocity, our algorithm is applicable to both TDD and FDD systems.

5 Conclusion

In this paper, we offered a strategy of subspace interference alignment for the cellular networks. We introduced the complex Grassmann manifold and derived a novel SD algorithm on this manifold to achieve perfect interference alignment. Moreover, different from most previous algorithms based on a joint design of precoder and receive filter, the proposed method achieves interference alignment with precoder design only. Thus it will significantly alleviate the overhead induced by alternating between the up and down links. Simulation results suggest that the proposed algorithm has better convergence performance and higher system capacity compared with previous methods. Finally we proved that the proposed algorithm converges monotonically.

References

[1] Cadambe V R, Jafar S A. Interference alignment and degrees of freedom of the K-user interference channel [J]. IEEE Transactions on Information Theory, 2008, 54(8): 3 425-3 441.

[2] Maddah-Ali M A, Motahari A S, Khandani A K. Signaling over MIMO multi-base systems: Combination of multi-access and broadcast schemes [C]// IEEE International Symposium on Information Theory. Seattle, USA: IEEE Press, 2006: 2 104-2 108.

[3] Jafar S A. Interference alignment: A new look at signal dimensions in a communication network [J]. Foundations and Trends in Communications and Information Theory, 2011, 7(1): 1-136.

[4] Suh C, Tse D. Interference alignment for cellular networks [EB/OL]. http://citeseerx. ist. psu. edu/viewdoc/download? doi = 10. 1. 1. 172. 5552&rep = rep1&type=pdf.

[5] Suh C, Ho M, Tse D. Downlink interference alignment[J]. IEEE Transactions on Communications, 2011, 59(9): 2 616-2 626.

[6] Yin H R, Ke L, WangZ D. Interference alignment and degrees of freedom region of cellular sigma channel [C]// Proceedings of the IEEE International Symposium on Information Theory. Petersburg, Russia: IEEE Press, 2011: 21-25.

[7] Zhang C, Li X, Yin H R, et al. Interference alignment precoder design on Grassmann manifold for cellular system[C]// First IEEE International Conference on Communications. Beijing, China: IEEE Press, 2012: 568-572.

[8] Gomadam K S, Cadambe V R, Jafar S A. Approaching the capacity of wireless networks through distributed interference alignment [C]// IEEE Global Telecommunications Conference. New Orleans, USA: IEEE Press, 2008: 1-6.

[9] Peters S W, Heath R W. Interference alignment via alternating minimization [C]// IEEE International Conference on Acoustics, Speech, and Signal

Processing. TaiPei, China: IEEE Press, 2009: 2 445-2 448.

[10] Kumar K R, Xue F. An iterative algorithm for joint signal and interference alignment [C]// IEEE International Symposium on Information Theory. Austin, USA: IEEE Press, 2010: 2 293-2 297.

[11] Liu S, Du Y G, Zhao M. A new joint iterative transceiver design with interference alignment method [C]// 19th Annual Wireless and Optical Communications Conference. Shanghai, China: IEEE Press, 2010: 1-5.

[12] Shen H, Li B. A novel iterative interference alignment scheme via convex optimization for the MIMO interference channel [C]// Vehicular Technology Conference. Ottawa, Canada: IEEE Press, 2010: 1-5.

[13] Shen H, Li B, Tao M X, et al. The new interference alignment scheme for the MIMO interference channe [C]// Wireless Communications and Networking Conference. Sydney, Australia: IEEE Press, 2010: 1-6.

[14] Ghauch H G, Papadias C B. Interference alignment: A one-sided approach [C]// IEEE Global Telecommunications Conference. Texas, USA: IEEE Press, 2011: 1-5.

[15] Santamaria I, Gonzalez O, Heath R W, et al. Maximum sum-rate interference alignment algorithms for MIMO channels [C]// IEEE Global Telecommunications Conference. Miami, USA: IEEE Press, 2010: 1-6.

[16] Edelman A, Arias T A, Smith S T. The geometry of algorithms with orthogonality constraints[J]. SIAM Journal on Matrix Analysis and Applications, 1999, 20(2): 303-353.

[17] Abrudan T E, Eriksson J, Koivunen V. Steepest descent algorithms for optimization under unitary matrix constraint[J]. IEEE Transaction on Signal Processing, 2008, 56(3): 1 134-1 147.

[18] 张贤达. 矩阵分析与应用[M]. 北京: 清华大学出版社, 2004.

[19] Hjørungnes A. Complex-Valued Matrix Derivatives: With Applications in Signal Processing and Communications[M]. Cambridge, UK: Cambridge University Press, 2011.

[20] AbsilP A, Mahony R, Sepulchre R. Optimization Algorithms on Matrix Manifolds[M]. New Jersey: Princeton University Press, 2008.

[21] Zhang C, Yin H R, Wei G. One-sided precoder designs for interference alignment [C]// IEEE Vehicular Technology Conference. Quebec, Canada: IEEE Press, 2012: 1-5.

[22] Manton J H. Optimization algorithms exploiting unitary constraints[J]. IEEE Transaction on Signal Processing. 2002, 50(3): 635-650.

[23] Boyd S, Vandenberghe L. Convex Optimization[M]. Cambridge, UK: Cambridge University Press, 2004.

[24] Polak E. Optimization: Algorithms and Consistent Approximations [M]. New York: Springer-Verlag, 1997.

[25] 王存祥, 邱玲. 协作多点传输中一种基于特征子信道的干扰对齐预编码矩阵优化方案[J]. 信号处理, 2011, 27(3): 395-399.